Numerical Modelling for the Distribution of ^{137}Cs and ^{131}I in the Scheldt Basin after a Potential Nuclear Accident

Amit Ravindra Patil[a,b*] (amit.ravindra.patil@sckcen.be), Fabricio Fiengo Perez[c] (fabricio.fiengo@aquafin.be), Jonathan Lambrechts[b] (jonathan.lambrechts@uclouvain.be). Insaf Draoui[b] (insaf.draoui@uclouvain.be) and Eric Deleersnijder[b,d] (eric.deleersnijder@uclouvain.be)

[a] *Belgian Nuclear Research Centre, Mol, Belgium.*

[b] *Institute of Mechanics, Material and Civil Engineering, Université catholique de Louvain, Louvain-la-Neuve, Belgium*

[c] *Aquafin, Aartselaar, Belgium*

[d] *Earth and Life Institute, Université catholique de Louvain, Louvain-la-Neuve, Belgium*

*Corresponding author: Amit Ravindra Patil; amit.ravindra.patil@sckcen.be

Numerical Modelling for the Distribution of ^{137}Cs and ^{131}I in the Scheldt Basin after a Potential Nuclear Accident

1 Introduction

Predictive models to develop environmental strategies for intervention are critical in making rapid decisions to minimize the potential impact of a nuclear accident. The contamination of water bodies, such as estuaries and rivers, after authorized liquid releases coming from nuclear installations does not represent a threat to the environment and human health due to relatively low levels of radioactivity. However, accidental releases such as those that happened during the Chernobyl disaster can become a concern. In Chernobyl, the radioactive contamination transported by the Pripyat river affected roughly 30 million people and eventually contaminated the Black Sea (IAEA, 2006a). The International Atomic Energy Agency (IAEA) has thus highlighted the need to have process-based models for radionuclide transport in regions that could be potentially affected by a nuclear accident (IAEA, 2019). The model simulations then provide useful information that allows efficient planning of human protection and environmental remediation measures.

Early experiences with the use of transport models for radionuclides can be found in the work of Prandle and Charnock (1997), who simulated the transport of dissolved ^{137}Cs from the Sellafield (UK) nuclear fuel reprocessing plant into the European Shelf Sea (Irish Sea) and similar work has been done for La Hague nuclear fuel reprocessing plant (Breton and Salomon, 1995). In the case of other facilities in Europe, such as the two nuclear power plants (NPPs, Doel and Borssele) in the Belgian-Dutch Scheldt Estuary (Figure 1), the use of models as assessment tools is a priority for the nuclear operators and national regulators. The tidal currents here are often strong, with a tidal range that can reach up to 5 m. Because of this, the contaminants can spread quickly upstream and downstream of the release point from the NPP.

Estuaries are subjected to marine influences such as tides, waves, and the influx of saline water and to fluvial influences such as flow of fresh water and sediments. Depending on the extent of these influences, the estuaries can be classified as high or low energy estuaries. High-energy or tide-dominated estuaries are dynamic ecosystems shaped by strong tidal energy at the mouth compared to wave energy (Reynaud et al., 2018). The tidal impact in these estuaries can reach hundreds of kilometers. Numerical modelling for radionuclide pollution transport in such high-energy estuaries is a challenging task because of the strong tidal currents with varying length and time scales (Periáñez et al., 2019). Although efforts have been made to develop marine radionuclide transport models (Brovchenko et al., 2022; Park et al., 2017; Periáñez et al., 2021; Periáñez and Cortés, 2023; Tsabaris et al., 2022), specific consideration must be given to tide-dominated estuaries. This is because it is important to deal with all the subdomains (rivers, sea, and estuary) simultaneously. This study focuses on the Scheldt estuary, which is representative of tide-dominated estuaries.

The Scheldt Estuary is a transitional zone with a unique ecosystem that is influenced by the Scheldt basin rivers and the currents of the North Sea. While the influence of the tides extends up to around 180 km upstream from the mouth of the estuary (van Rijn, 2013), the rivers still affect the near-shore dynamics of the Scheldt Estuary (Lacroix et al., 2004). Therefore, to simulate the fate of radionuclides in the Scheldt estuary, it is necessary to represent the circulation patterns in

the European shelf region and the river hydrodynamics. However, the simulation of such a system is complex due to its multiscale nature (e.g., river, estuary, coast, and sea).

The contamination of water systems during an accident is not restricted to direct radioactive liquid releases from nuclear installations but also due to atmospheric releases in the form of radioactive wet and dry deposition. In past nuclear accidents, in addition to direct releases into the ocean, wet and dry depositions resulted in a significant amount of radioactivity in aquatic systems (Kawamura et al., 2011; Kobayashi et al., 2013; UNSCEAR, 2021). Besides the circulation patterns and the release pathways, the characteristics of the source term (radioactive composition of the release) are also important. It was found that ^{137}Cs and ^{131}I were important contributors for short-term radiation exposure to humans in both the Fukushima (UNSCEAR, 2021) and Chernobyl accidents (IAEA, 2006b). ^{137}Cs is a non-conservative radionuclide due to its adsorption property on sediments, and given its long half-life of 30 years, it can linger in the ocean for years (Behrens et al., 2012; Estournel et al., 2012; Prandle and Charnock, 1997; Tsumune et al., 2012).

This study introduces a computational model for simulating ^{137}Cs and ^{131}I transport in the Scheldt basin (estuary, river, and European Shelf region). In this framework, two-dimensional shallow water equations are coupled with section-averaged river models. The model includes the advection by the currents and river flow, turbulent mixing in the estuary, and radioactive decay. The model is then employed for the simulation of radionuclide transport under hypothetical scenarios for radioactive releases from the Doel NPP located on the bank of the estuary. The scenarios in this study are chosen in such a way that they lead to a worst-case release condition in the Scheldt environment.

2 Materials and Methods

2.1 Model Domain

The upstream limits of the model domain were defined based on the location of hydrometric stations in order to use discharge information for the definition of boundary conditions in the model. Most of these stations are located upstream, at the end of the tidal zone for the Scheldt basin. The downstream boundary of the model coincides with the shelf break in the North Atlantic Ocean. The boundary in the sea was placed far away from the area of study to minimize its influence on simulations. This is because the hydrodynamic conditions along the sea boundary obtained from global tidal models can become inaccurate as they approach the shallow regions (de Brye et al., 2010).

The entire system of the Scheldt includes rivers, estuary, and the European continental shelf (herein referred to as the shelf region). The representation of such a system in a model involves a multiscale approach (Figure 1). In this regard, the domain was divided into two regions: the first region is the tidal Scheldt rivers and their tributaries, and the second is the Scheldt estuary and the shelf region.

The first region comprises (1) the tidal part of the Scheldt River, which extends from Ghent to the Hemiksem, with a width increasing from 50 m at Ghent up to around 500 m at the Hemiksem and (2) the tributaries of the Scheldt: the Durme, Rupel, Dyle, Kleine Nete, Grote Nete, and Zenne (widths from 10 m). Since the variation of the hydrodynamic variables across the river

section can be neglected for the rivers inside the first region, we use the one-dimensional section averaged equations for the representation of flow and transport. The second region extends from Hemiksem (just after the confluence with Rupel) until the shelf break. The mouth of the estuary is roughly 8 km wide at Vlissingen. In this region, the flow circulation is predominantly two-dimensional. The measurements inside the estuary show that during flood and ebb tides, the water flows through different pathways. Therefore, in this region, the simulation of flow and transport is done by using two-dimensional depth-averaged equations. To represent a continuous transition between the rivers and the estuary-sea, both regions are connected.

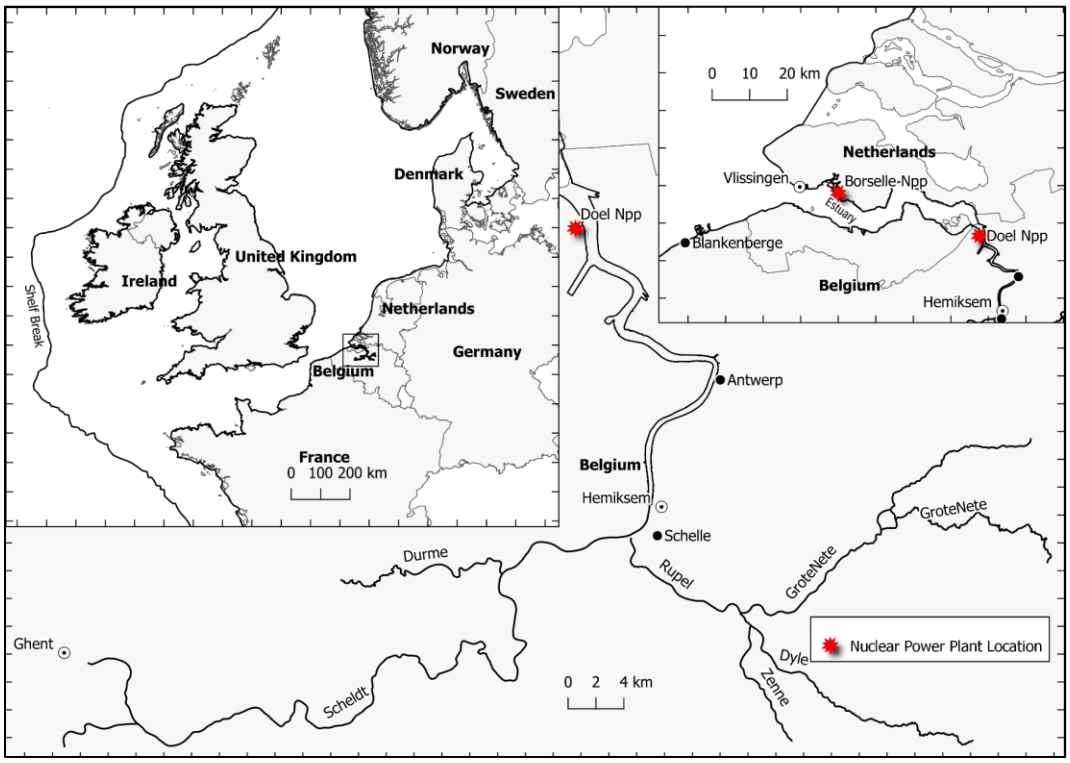

Figure 1. Model domain for the one-dimensional region that includes the Scheldt River (from Ghent to Hemiksem) and its tributaries, along with the two-dimensional region that includes the Scheldt Estuary (from Hemiksem to Vlissingen) and the Shelf Region, with the location of NPPs.

2.2 Coupled Hydrodynamics Module

In the first region, the Saint-Venant equations are formulated in terms of discharge (Q) and cross-sectional area (A) in Eq. 1-2:

$$\frac{\partial A}{\partial x} + \frac{\partial Q}{\partial x} = 0 \tag{1}$$

$$\frac{\partial Q}{\partial t} + \frac{\partial}{\partial x}\left(\frac{Q^2}{A} + \frac{P}{\rho}\right) = gA\frac{\partial h}{\partial x} - gS + \frac{F}{\rho} \tag{2}$$

Where t is the time, x is the spatial coordinate along the river, g is the acceleration due to gravity, h is the water depth to the deepest point in cross section, ρ is the water density, P is the hydrostatic pressure force, F is the along-flow component of the pressure force resulting from the width variation, and S is a frictional term estimated according to the Manning formula, i.e.,

$$S = n^2 \frac{Q|Q|b^{*4/3}}{(A)^{7/3}} \quad (3)$$

In the above relation, n is the Manning coefficient and b^* is the free surface width. The cross-section A depends on the riverbed elevation profile and the free water surface level (η) at position x. The domain is divided into line segments, and the solution is then discretized at each elemental node. On each node of the discretized elements, the cross-section profile for the rivers is extracted from the bathymetric data collected by 'Flanders Hydraulic Research'. Hourly discharge measurements are applied to the upstream node boundary of each river. At the confluence points of the rivers, a bifurcation solver is used. The existing hydraulic works are also included in the discretization, and they consider the changes in direction and different submersion conditions.

The second component of the domain is simulated using two-dimensional depth-averaged equations. The shallow water equations here are formulated in terms of the velocity ($\boldsymbol{u}$) and the actual water depth (H) at a position of x and y in Eq. 4-5:

$$\frac{\partial U}{\partial t} + \nabla.\mathrm{F(U)} = G(U) \quad (4)$$

Where,

$$U = \begin{bmatrix} \eta \\ Hu \\ Hv \end{bmatrix}, F(U) = \begin{bmatrix} Hu & Hv \\ Hu^2 + g\frac{H^2}{2} - Hv\frac{\partial u}{\partial x} & Huv - Hv\frac{\partial u}{\partial y} \\ Huv - Hv\frac{\partial v}{\partial x} & Hv^2 + g\frac{H^2}{2} - Hv\frac{\partial v}{\partial y} \end{bmatrix}, \quad (5)$$

$$G(U) = \begin{bmatrix} 0 \\ -g\tau_x + gH\frac{\partial h}{\partial x} + fv \\ -g\tau_y + gH\frac{\partial h}{\partial y} - fu \end{bmatrix}$$

$\boldsymbol{u} = (u, v)$ is the depth averaged horizontal velocity, υ is the horizontal eddy viscosity, f is the Coriolis factor, and τ is the bed shear stress as represented in Eq. 6.

$$\tau = n^2 \frac{H\boldsymbol{u}|H\boldsymbol{u}|}{(H)^{7/3}} \quad (6)$$

where n is the Manning coefficient. The domain here is represented by an unstructured mesh consisting of triangular elements (28,000 triangular elements), as presented in Figure 2. Since the domain of interest is the Scheldt estuary, a finer mesh is used in the upper estuary and the southern bight of the shelf area (Belgian Coastal Region) (Figure 2b). Here, elements with a maximum width of 750 m are used. For shallower regions, such as the lower estuary, the maximum width size of the elements is around 100 m (Figure 2c). Since computational time is of importance, the mesh size is optimized. The bathymetry of the region was obtained from European marine observation and data network (EMODnet). The boundary conditions imposed at the shelf break were obtained from the simulations of elevation and velocity harmonics done by the global ocean tidal model (TPXO9.1) (Egbert and Erofeeva, 2002). For the meteorological forcing, wind velocities (10 m above sea level) were obtained from the Copernicus climate database (Hersbach et al., 2020).

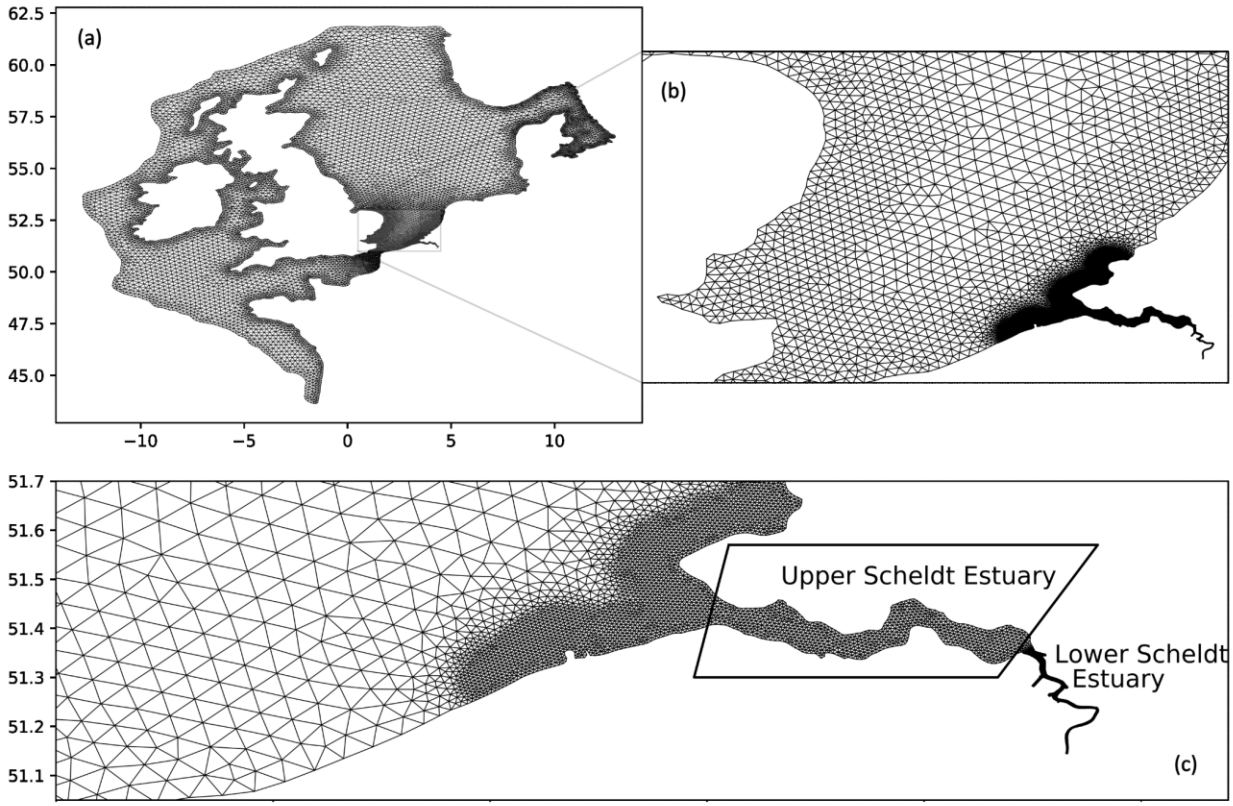

Figure 2. (a) Unstructured triangular mesh generated for the discretization of a two-dimensional section of the model domain, (b) with higher mesh resolution in the upper and (c) lower estuary.

For the connection between regions, a boundary-connected coupling based on flux continuity is adopted. The hydraulic structures are implemented by using a flux term that allows to represent the stage-discharge relationship in the discontinuous Galerkin (DG) method. The whole system of equations is then solved using the DG method of the SLIM (Second Generation Louvain-la-Neuve Ice Ocean Model, www.slim-ocean.be) modelling framework (Bladé et al., 2012; Draoui et al., 2022, 2020; Patil et al., 2022). Supplementary material contains a discussion of the model's calibration and performance in the shelf region, coast, estuary, and river compared to field measurements.

2.3 Transport Module

2.3.1 Radionuclide Model: ^{137}Cs and ^{131}I

Radionuclide transport (^{137}Cs and ^{131}I) is simulated using a Eulerian approach including advection, diffusion and radioactive decay. ^{137}Cs has a half-life of 30 years, while that of ^{131}I is just 8 days. The corresponding transport equations are as follows:

For 1D domain

$$\frac{\partial Ac}{\partial t} + \frac{\partial}{\partial x}(Qc) = \frac{\partial}{\partial x}\left(DA\frac{\partial c}{\partial x}\right) + S - \lambda Ac \tag{7}$$

For 2D domain $$\frac{\partial Hc}{\partial t} + \nabla.(H\boldsymbol{u}c) = \nabla.(HD\nabla.c) + S - \lambda Hc$$

where S is the source for the radionuclide under consideration and λ is the decay constant of the radionuclide. The source term S here is used to define radioactive fallout or direct liquid releases. In the model, it is assumed that the radionuclides that enter the simulation domain are well mixed in the element where the release point is located. Other processes, such as biological and suspended sediment adsorption, are excluded. This assumption is valid for accidental releases where the duration of the simulation period is short, or in the case of radionuclides such as ^{131}I that do not tend to readily adsorb themselves to the sediments (Periáñez et al., 2019). Studies have shown good agreement when ignoring such effects (i.e., adsorption on sediments) under these circumstances (Tsumune et al., 2012). However, this assumption does not hold for long-term simulation where accumulation, settling, and resuspension play a significant role for radionuclides such as ^{137}Cs. It is also worth noting that the adsorption property of ^{137}Cs to the sediment decreases significantly if the salinity increases (Wang et al., 2022).

2.3.2 Salinity Model

The salinity model is simulated using the same set of equations as the radionuclide transport model, with the exception that the decay term is dropped and the source term is restricted to just saline liquid releases. The simulation units are expressed as practical salinity units (PSU). The changes in salinity caused by biological or chemical interactions can be neglected. Salinity is, thus, referred to as a conservative quantity that is merely transported by advection and diffusion processes and hence provides a good tracer of water masses. Furthermore, due to the available measurements of this variable, salinity becomes an ideal choice for the verification of the transport model.

In the model, the entering salinity of the river and its tributaries is set to zero. For inflow periods, the salinity at the shelf break boundary is prescribed to be 35, which corresponds to an average of climatology data and measurements (Lacroix et al., 2004). The initial condition in the model is a linear salinity profile in the estuary that extends from the point of zero salinity observed in the Scheldt River near Hemiksem to the Belgian shore at a salinity of 35. In the rest of the shelf region, a uniform salinity level of 35 is used as the initial condition, with zero salinity in the rivers and tributaries. The supplementary material contains the salinity simulation results of this model and their comparison to measurements.

2.4 Hypothetical Scenario Definition

2.4.1 Releases and source term definition

We are interested in using this model to evaluate the impact of accidental releases coming from the Doel NPP into the Scheldt estuary. The Doel NPP is located on the banks of the Scheldt estuary near Antwerp (Belgium) at $51^0$2' N and $4^0$2' E (Figure 1). The source term (radionuclide composition) is restricted to ^{137}Cs and ^{131}I. These two radionuclides were selected based on the values established in the Fukushima accident. Several hypothetical accidents occurring at the Doel NPP were considered and simulated. These scenarios are selected in order to have worst case conditions after atmospheric and direct releases in the Scheldt basin. The amount of radionuclides that are hypothetically released from the Doel NPP in this study is based on the Fukushima accident as reported by UNSCEAR (2021) (Table 1).

Table 1 Total radionuclide releases as reported by UNSCEAR (2021) from the Fukushima accident to the atmosphere and as a direct release pathway into the aquatic environment.

Pathways	Total Release (PBq)	
	^{131}I	^{137}Cs
Atmospheric deposition	100-500	6-20
Direct release (March – April 2011)	9-13	3.5-5.6

For the atmospheric deposition source, the JRODOS atmospheric model (Raskob et al., 2016) was used to determine the activity distribution of ^{137}Cs and ^{131}I on the surface of the Scheldt basin. The JRODOS model has been previously utilized for assessments following the Fukushima accident (Ievdin et al., 2012; Kovalets et al., 2014; Selivanova et al., 2023). For this study, the radioactivity deposition results were obtained after an atmospheric release period of 6 hours. The release period is based on observations from the Fukushima accident which show that most of the release to atmosphere occurs within this timeframe (Tsuruta et al., 2014).

2.4.2 Meteorological conditions of the study area

The water currents and meteorological conditions of the Scheldt Estuary are quite variable. For our purpose, we consider a realistic combination of conditions that could deliver the maximum impact. Therefore, the simulation period starts on the first day of July (the summer period), when, on average the freshwater flows are low (the dry period). Moreover, the winds (Northwest winds) in the shelf region and water currents are generally more regular than in other seasons (Hossen and Akhter, 2015). During this period, the wind speed over the estuary can range from 0 up to 3-4 m/s (Hossen and Akhter, 2015). In the Scheldt estuary, the maximum frequency in a year for wind direction occurs between 180^0 – 300^0 (180^0 is in the south direction) (Hossen and Akhter, 2015). That indicates that in a possible scenario of accidental release, there is a higher probability that the atmospheric release plume will move towards the sea; moreover, the lower wind velocities would result in a highly concentrated deposition of radionuclides.

There are many possible combinations of wind speed and direction that could occur at the moment of an accident. We considered two specific meteorological conditions: (1) atmospheric releases are directed towards the lower estuary, rivers, and tributaries; and (2) the release is towards the sea. Figure 3 shows the area of deposition for radionuclides considered in the scenarios, and Table 2 presents the parameters used for them.

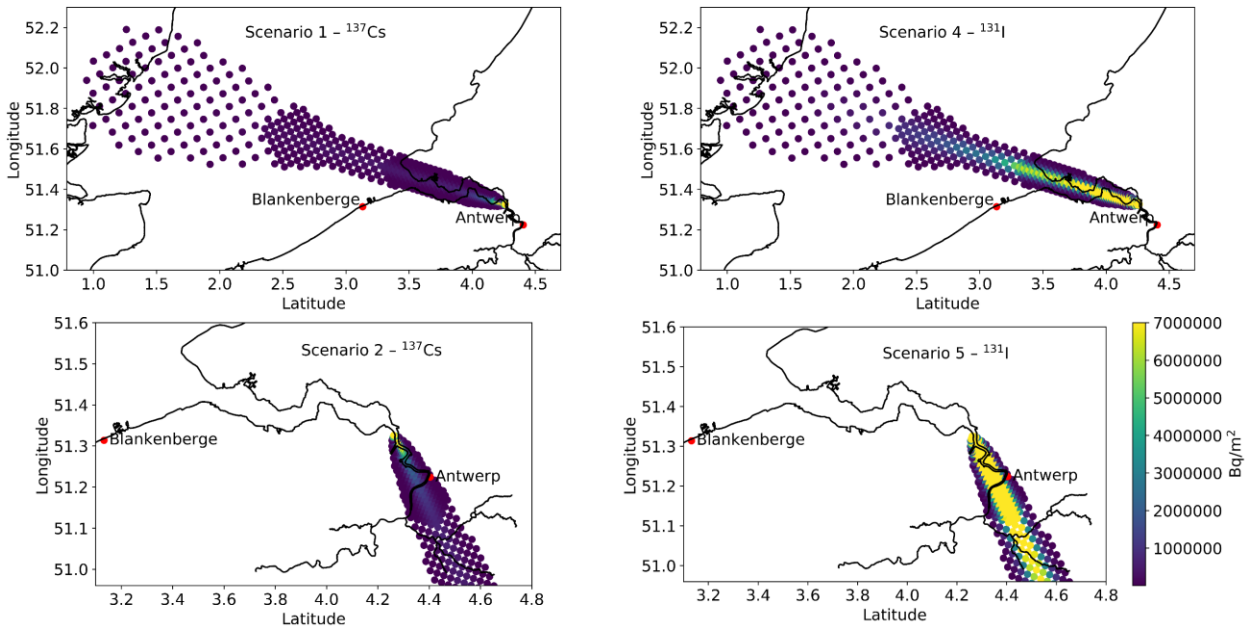

Figure 3. Total amount of radionuclide deposited on the Scheldt basin after 24 hours of initial release as computed by the JRODOS model for ^{137}Cs and ^{131}I and two wind directions for scenarios 1,2,4 and 5.

Table 2 Scenario definitions for ^{137}Cs and ^{131}I and their amount of radioactivity released in the Scheldt basin for the model.

Scenario	Radionuclide	Pathways	Amount released	Wind Speed	Wind direction
1	^{137} Cs	Atmospheric depositions	10 PBq	1 m/s	290^0 WNW
2					135^0 SE
3		Direct Release	52 GBq/min		
4	^{131}I	Atmospheric depositions	100 PBq	1 m/s	290^0 WNW
5					135^0 SE
6		Direct Release	127 GBq/min		

The liquid radioactivity released directly into the estuary during the scenarios presented in Table 2 is based on the releases that occurred during the Fukushima accident. As reported, it was very difficult to estimate the duration of the accidental release of radionuclides that occurred by using backward extrapolation of inventories (UNSCEAR, 2021). Here, we assume an accidental release scenario of six hours to keep the combination of atmospheric and direct liquid release. The rate of release is estimated from the total amount of radionuclide released between March and April 2011, with inventories of ^{137}Cs at 5 PBq and ^{131}I at 12 PBq (UNSCEAR, 2021). The simulation period considered here is about a month after the initial release since the model is developed with the aim to catch the peak activity concentration and to guide the actions to be taken during and immediately after the accident. In case of longer periods, measurements of activity are feasible and more reliable (Cao et al., 2022).

2.4.3 Hydrodynamic conditions

The scenarios presented in Table 2 involve radioactive release from different pathways and meteorological conditions. Here, we consider the effects of the hydrodynamics in the Scheldt basin on the distribution of radioactivity. For this, we consider two cases: (1) the influence of

releases starting at high and low tide (at the point of release); and (2) seasonal differences between the months of January and July. The Scheldt estuary is greatly influenced by tides; thus, the tide conditions at the start of release can play a role in the distribution of the radioactivity. For instance, if the plume is released during low tide, it is likely to move towards inland regions in the first six hours. During the wet season additional fresh water is delivered in the Scheldt basin and this could potentially alter the activity levels as well as the spatial distribution. Therefore, the model is simulated for January, which has more rainfall and storm surges than July. For all the scenarios discussed here, we use the conditions indicated in scenario 1, which involves ^{137}Cs.

3 Scenario Simulations: Results

The simulation results for activity concentration of radionuclides under the scenarios discussed in Section 2.4 are presented in this section. The simulation results were acquired using a computer with i7 8th generation CPU and 16 GB RAM which takes around 24 hours for a 7-day simulation period.

3.1.1 Atmospheric Releases: Scenario 1 and 4

Figure 4a and 4c show the activity concentration of ^{137}Cs and ^{131}I respectively, after 76 hours (~3 days) of release and Figure 4b and 4d show the concertation after 25 days of release.

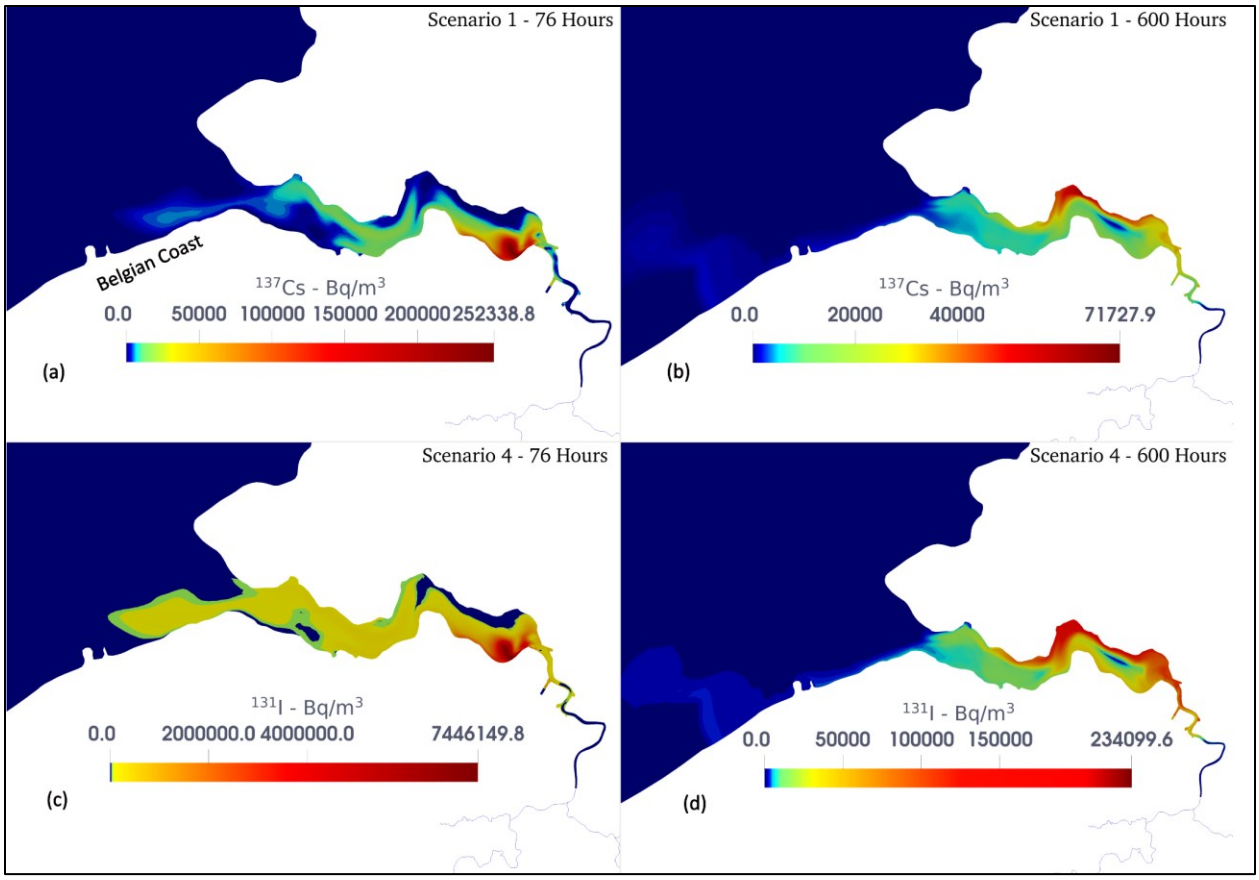

Figure 4. Simulated radionuclide concentrations in surface waters (a) after 3 days of initial release for ^{137}Cs, (b) after 25 days of initial release for ^{137}Cs as defined in scenario 1, (c) after 3 days of initial release for ^{131}I, and (d) after 25 days of initial release for ^{131}I for scenario 4.

The concentration of ^{131}I is substantially higher than that of ^{137}Cs, particularly in the initial days following the release. This larger initial concentration occurs because the overall amount of ^{131}I emitted is ten times higher than that of ^{137}Cs. In this scenario, where the atmospheric release is directed towards the coast, the plume in the estuary moves to the Belgian coast. This is expected due to the tidal motion known for this estuary (Lacroix et al., 2004). The concentration of ^{131}I at the coast is higher than 10 kBq/m^3. While for ^{137}Cs, the concentration never exceeds this value. Figure 5 shows the concentration of both radionuclides at the location of Blankenberge (for location, see Figure 1). It is evident that in the coastal region the release of ^{131}I has a greater impact than the release of ^{137}Cs, but the maximum concentration (>10 kBq/m^3) for ^{131}I is not expected to reach until seven days following the first release.

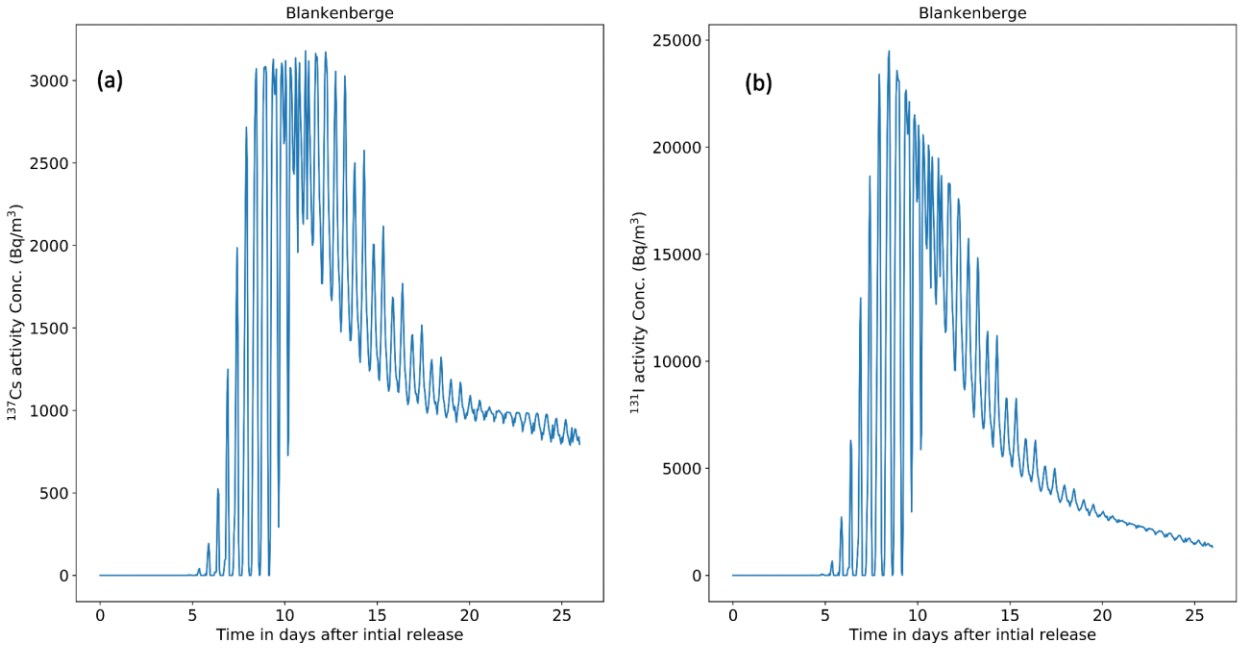

Figure 5. Temporal variation of activity concentrations at Blankenberge located at the Belgian Coast: (a) ^{137}Cs for model parameters defined in scenario 1 and (b) ^{131}I for model parameters defined in scenario 4.

Since ^{131}I decays faster than ^{137}Cs, the concentration starts to decline soon after reaching the peak value at about nine days, after which the concentration drops below 10 kBq/m^3 (at about 16 days after the initial release). Moreover, Figure 5 shows the ^{131}I concentration is comparable to the ^{137}Cs concentration at around 25 days. For ^{137}Cs, the decrease in concentration is seen due to the water influxes from the English Channel from the south-east towards the Southern Bight region (i.e., the Belgian Coast). Therefore, in the case of ^{131}I too, the dilution could be an additional reason for the decrease in concentrations.

After a nuclear accident, the Scheldt Estuary would be most affected by atmospheric deposition because of its proximity to the NPP. It is worth mentioning that the maximum concentration of these radionuclides is present near the mouth of the lower estuary (i.e., downstream the Doel NPP). Even though the release is towards the coast, the tidal motion in the estuarine part transports the radionuclides towards the inland basin. Antwerp city (Figure 1), located upstream from the NPP, is an important urban and industrial settlement that is expected to be the most

affected by these releases. Figure 6 shows the temporal variations of the concentration at Antwerp.

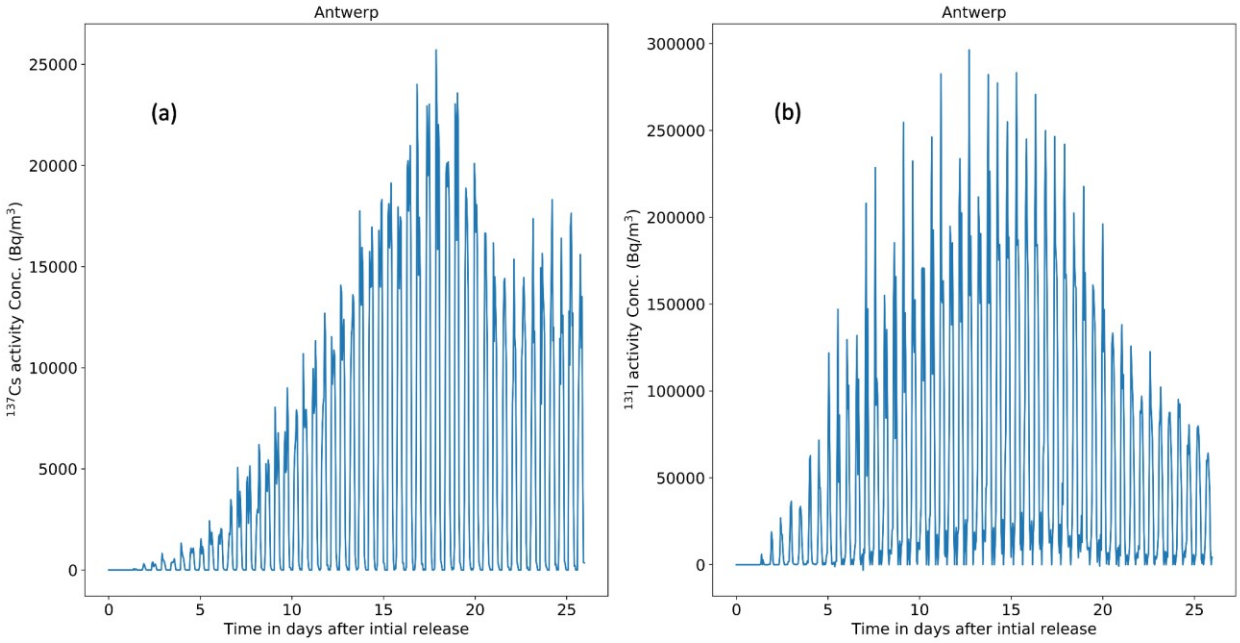

Figure 6. Temporal variation of activity concentrations at Antwerp located at the Scheldt estuary: (a) ^{137}Cs for model parameters defined in scenario 1 and (b) ^{131}I for model parameters defined in scenario 4.

Figure 6 shows that the tidal motion brings a significant amount of radioactivity towards upstream parts of the estuary. Though both radionuclides exceed zero in around two days, the ^{131}I exceeds 10 kBq/m^3 only after three days and the ^{137}Cs after ten days of release from the NPP. Maximum concentrations occur around the 12th and 18th day for ^{131}I and ^{137}Cs, respectively. However, the backward motion of the radioactive plume never goes beyond Hemiksem in the inland river basin.

3.1.2 Atmospheric Releases: Scenario 2 and 5

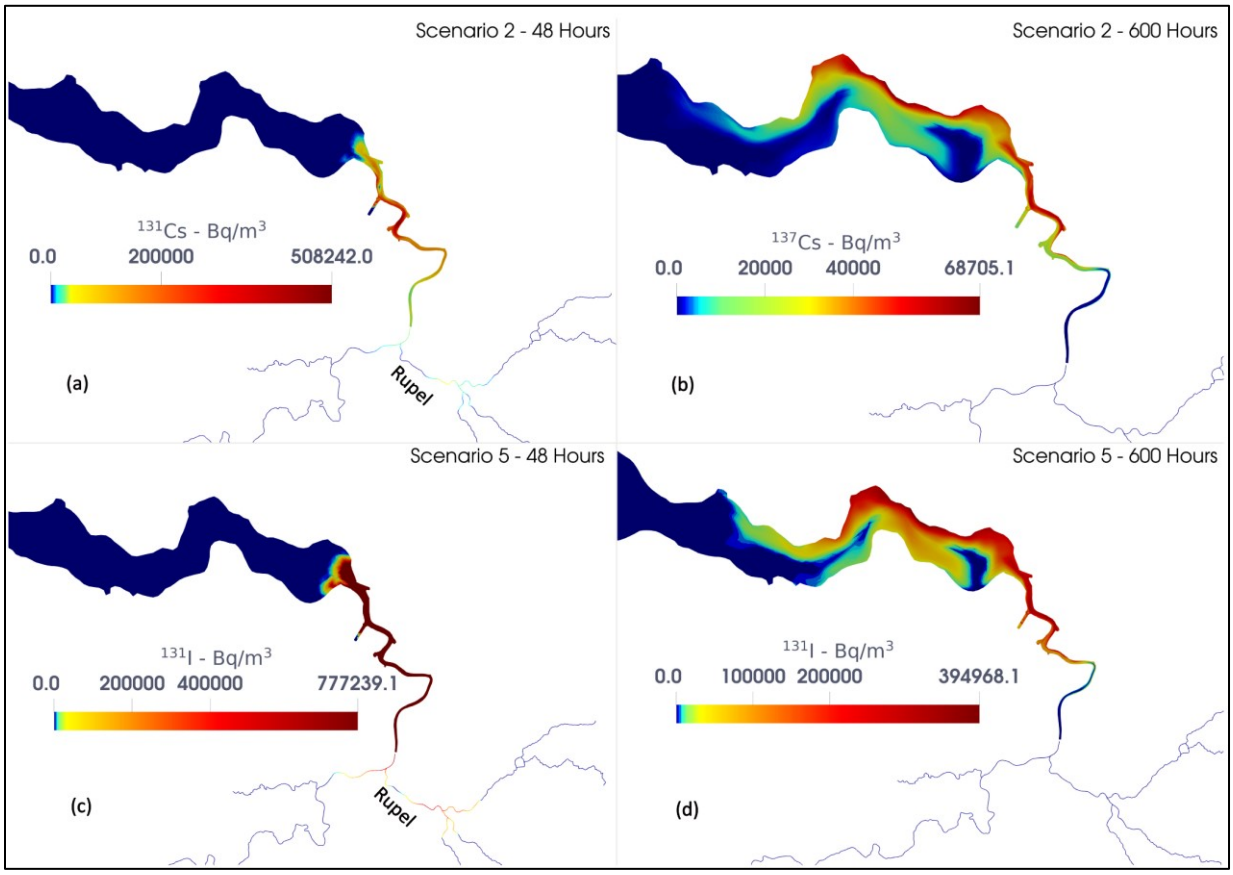

Figure 7. Simulated radionuclide concentrations in surface waters (a) after 2 days of initial release for ^{137}Cs, (b) after 25 days of initial release for ^{137}Cs as defined in scenario 2, (c) after 2 days of initial release for ^{131}I, and (d) after 25 days of initial release for ^{131}I for scenario 5.

Figure 7a and 7c show the concentration of ^{137}Cs and ^{131}I after 48 hours. This shows that the deposited plume on the far reach of tributaries moves faster downstream towards the confluence with the Rupel River. This is primarily because freshwater dynamics can become dominant towards the upstream reach of the tributaries, thus decreasing the flushing time. Nonetheless, even if the plume moves downstream faster (within 3-4 days) towards the mouth of the Rupel River (Figure 7a and 7c), it takes roughly 6 days for ^{137}Cs and 19 days for ^{131}I to reach lower activity levels (<10 kBq/m^3) in Rupel. This is because ^{131}I is released in greater quantities than ^{137}Cs. But it is essential to note that larger depositions in the tributaries would result in a longer period of radioactive contamination in the Rupel River. Figure 7b and 7d show the distribution for ^{137}Cs and ^{131}I after 25 days of release. In this case, the activity concentration is spread in the estuary and no activity is predicted in the coast.

Figure 8 shows the concentration of radionuclides in tributaries right before their confluence with the main rivers which are: the Dyle River connected to Rupel (Figure 8a and 8b), the Grote Nete connected to Rupel (Figure 8c and 8d), and then the Rupel connected to the Scheldt River (Figure 8e and 8f).

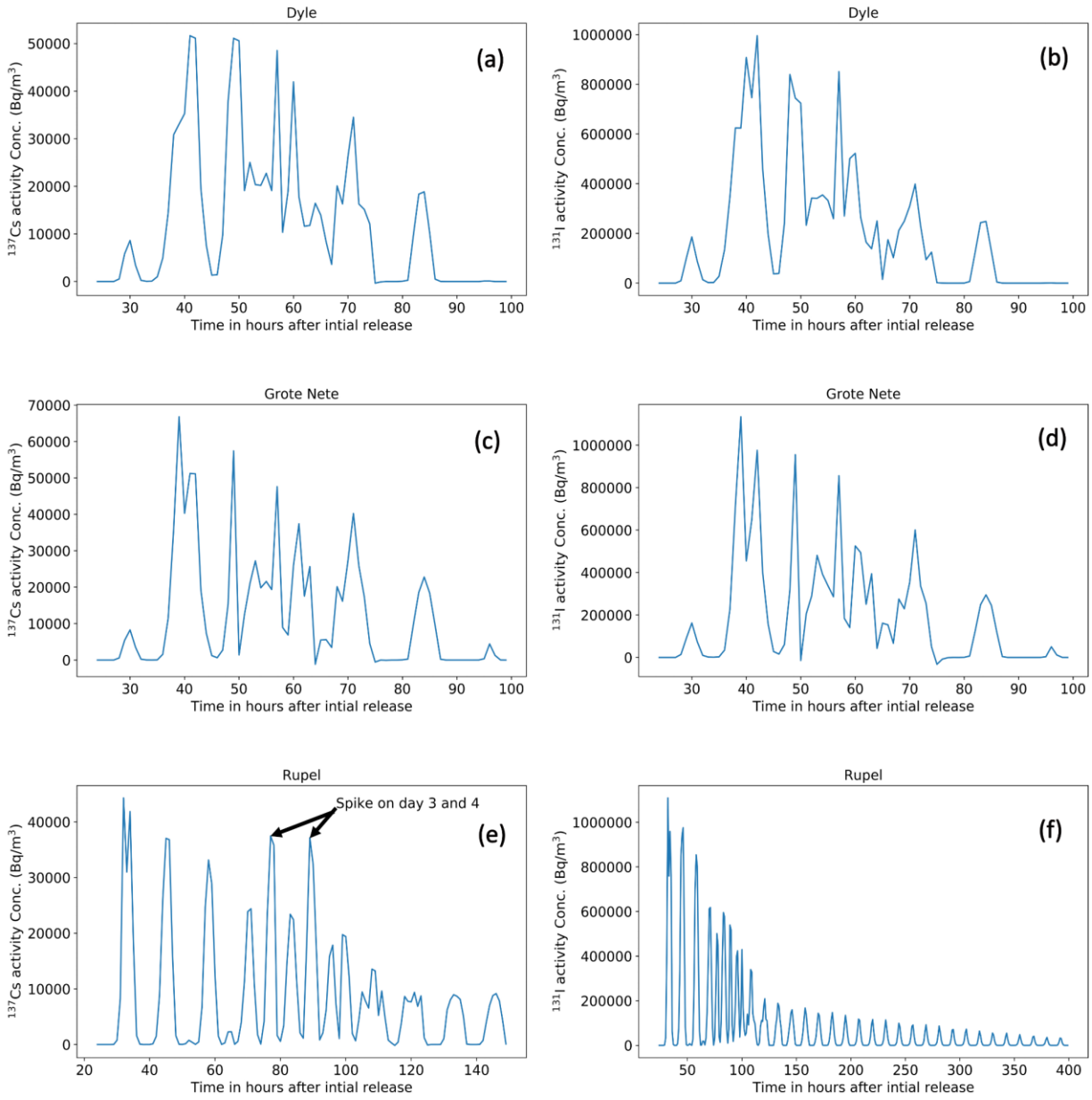

Figure 8. Temporal variation of concentrations in the tributaries of the Scheldt River: (a) ^{137}Cs and (b) ^{131}I in the Dyle River for scenarios 2 and 5 respectively, (c) ^{137}Cs and (d) ^{131}I in the Grote Nete River for scenarios 2 and 5 respectively and (e) ^{137}Cs and (f) ^{131}I in the Rupel River for scenarios 2 and 5 respectively. The extracted concentration is located immediately before the confluence with the main river.

It is important to note that the confluence of the Rupel with the Scheldt River is approximately 12 km downstream from the beginning of the Rupel River (the confluence point of the Nete, Dyle and Zenne rivers). In the tributaries of the Rupel, the radionuclide plume stays for approximately 4 days, but the concentrations reach significant quantities of up to 70 kBq/m^3 in the case of ^{137}Cs and 1 MBq/m^3 for ^{131}I. In the Rupel River, two activity hot spots are noticeable. One coming from upstream, transported by the water from its tributaries and another from downstream, transported by the tidal motion. This is clearly presented in Figure 7c, where the separated plumes coming from the estuary (downstream) and its tributaries (upstream) are

visible. As seen by the spikes in Figure 8e between days 3 and 4, both the plumes join in the Rupel River and travel towards the estuary.

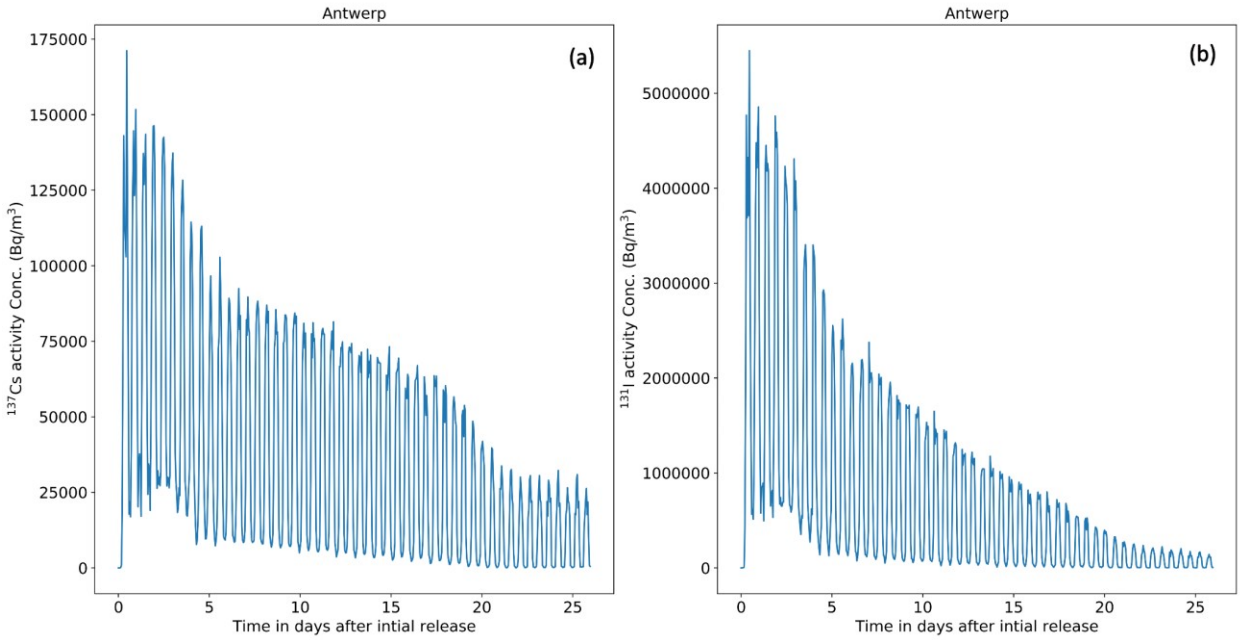

Figure 9. Temporal variation of concentrations at Antwerp located at the Scheldt estuary: (a) ^{137}Cs for model parameters defined in scenario 2 and (b) ^{131}I for model parameters defined in scenario 5.

Figure 9 shows the activity concentrations of both radionuclides at Antwerp, showing that it is once again one of the most vulnerable locations in this scenario. Moreover, since the atmospheric releases deposit on the surroundings of Antwerp, the rise in concentration to its maximum value is almost immediate and is also higher compared to scenarios 1 and 4. Since inland depositions also reach these areas, as described in scenarios 2 and 5, they have the greatest effect in this location. The concentration of ^{131}I after the end of the simulation period is around 125 kBq/m^3, and that of ^{137}Cs is 30 kBq/m^3.

3.1.3 Direct liquid releases: Scenario 3 and 6

The distribution of ^{137}Cs and ^{131}I in surface water for direct release scenarios 3 and 6 is shown in Figure 10. Figure 10a and 10c show the activity concentrations of ^{137}Cs and ^{131}I, respectively, after 72 hours (~3 days) of release, and Figure 10b and 10d show the concentrations after 25 days of release.

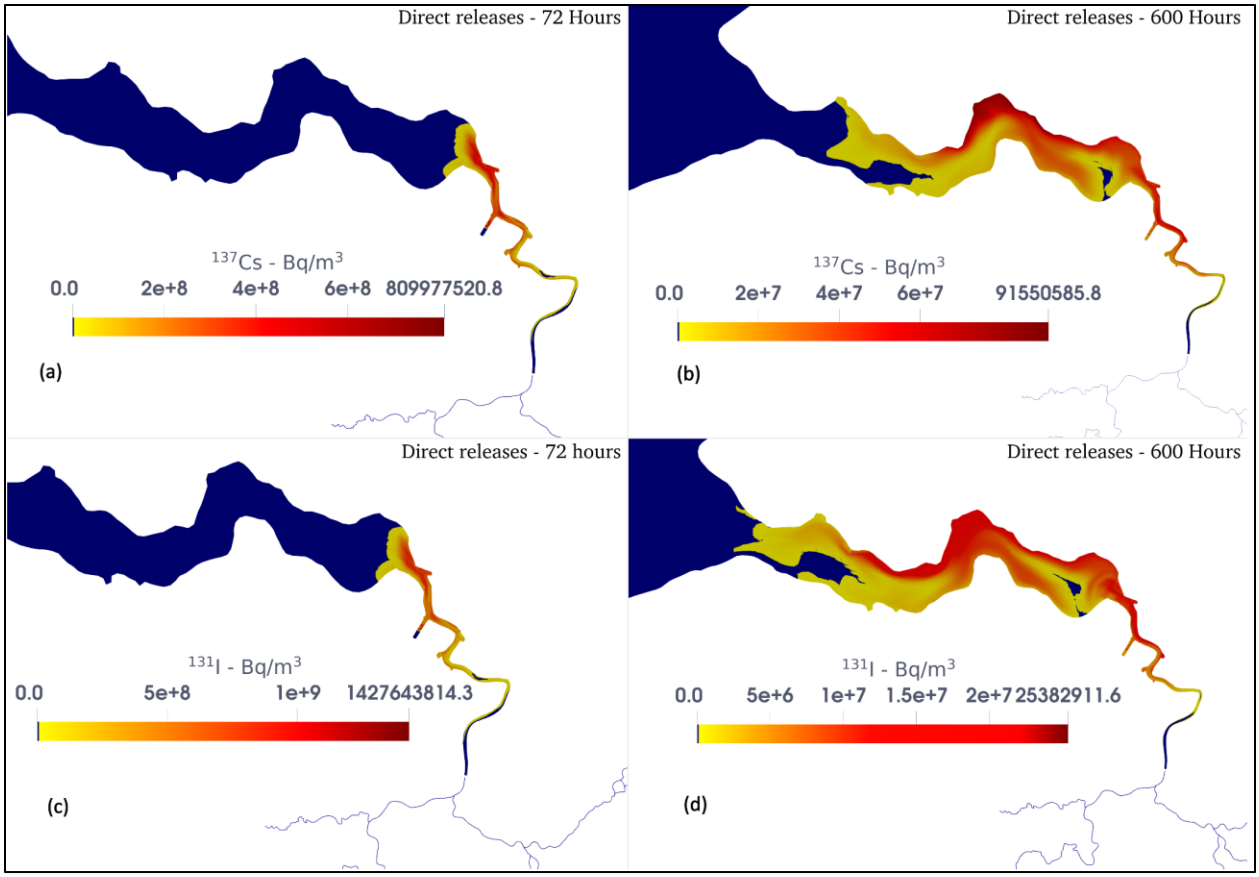

Figure 10. Simulated radionuclide concentrations in surface waters (a) after 3 days of initial release for ^{137}Cs, (b) after 25 days of initial release for ^{137}Cs as defined in scenario 3, (c) after 3 days of initial release for ^{131}I, and (d) after 25 days of initial release for ^{131}I for scenario 6.

The direct liquid release scenarios are treated as point source releases into the Scheldt estuary that are subjected to advection and dispersion. Since the transport in the estuary is dominated by advection, the extent of the affected areas after three days of release for both radionuclides is comparable. Even if ^{131}I has a one-order-of-magnitude higher release rate, the concentrations of both radionuclides after about a week become equivalent in magnitude. This can be observed at Antwerp, where the concentration becomes similar after about 8 days of release. Later, the concentration of ^{131}I starts decreasing considerably (Figure 11).

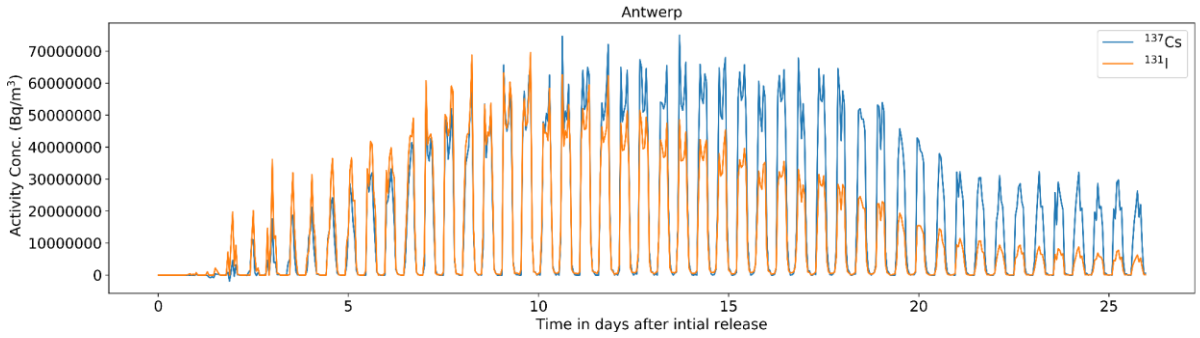

Figure 11. Temporal variation of concentrations at Antwerp located at the Scheldt estuary: ^{137}Cs for model parameters defined in scenario 3 and ^{131}I for model parameters defined in scenario 6.

About a month after the release, the extent of affected areas for both radionuclides is comparable (Figure 10c and 10d). The total inventory released in these scenarios is 45.72 TBq of ^{131}I and 1.8 TBq of ^{137}Cs. Even though these are considerably smaller than the atmospheric releases (Table 2), it must be kept in mind that only a portion of what is released is deposited on the Scheldt. While in the event of a direct release, the total inventory is released. That leads to concentrations that are considerably higher (>10 kBq/m^3) and the maximum concentration at Antwerp has a greater peak than in other scenarios. It is important to emphasize that following the initial release, the entire lower estuary becomes contaminated within a few days and begins to spread in the upper estuary. As seen in Figure 10a and 10b, both radionuclides reach the mouth of the estuary approximately 25 days after discharge. However, compared to ^{137}Cs, the concentration of ^{131}I has now decreased. This is visible when the scale of the figures is kept the same for both radionuclides, as shown in Figure 12a and 12b.

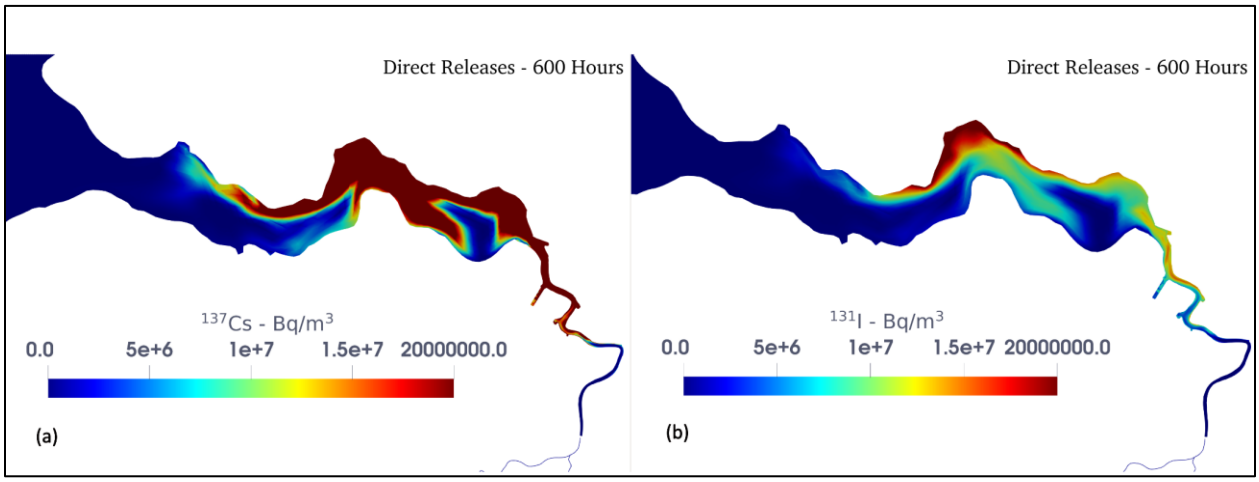

Figure 12. Simulated radionuclide concentrations in surface waters (Bq/m^3) (a) after 25 days of initial release for ^{137}Cs, (b) after 25 days of initial release for ^{131}I as defined in scenarios 3 and 6 respectively. Both figures are equally scaled to a maximum of 20 MBq/m^3 to show thet impact of degradation in the case of ^{131}I.

Under these scenarios, the radioactive plume in the Scheldt River propagates upstream until about the mouth of the Durme and the Rupel River. Furthermore, the extent of affected areas toward inland rivers appears to be greater in scenarios 3 and 6 than in the others (liquid releases vs atmospheric releases). Figure 13a and 13b show the concentration of ^{137}Cs and ^{131}I at the location of Schelle (see Figure 1 for location) for the different scenarios.

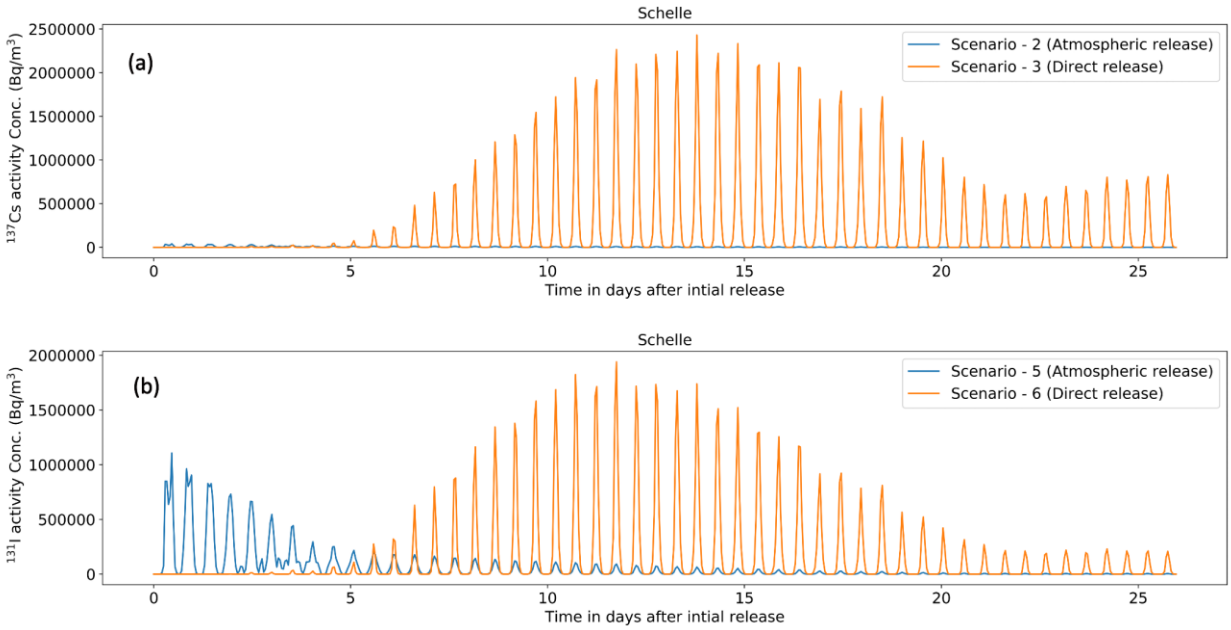

Figure 13. Temporal variation of concentrations at Schelle located in the Scheldt River: (a) ^{137}Cs for model parameters defined in scenarios 2 and 3 and (b) ^{131}I for model parameters defined in scenarios 5 and 6.

For scenarios 1 and 4, which involve radioactive deposition towards the coast, there is no significant impact at Schelle and are thus excluded from Figure 13. Moreover, as shown in Figure 13, the impact of ^{137}Cs and ^{131}I in the case of atmospheric releases are lower than those of direct releases. However, scenario 5 and, even to a smaller extent, scenario 2 have an impact at this location that occurs earlier. Whereas the concentration in the direct release scenario stays low for up to 4-5 days. The peak of ^{131}I occurs on the 12th day after release, followed by the peak of ^{137}Cs two days later. Figure 13 shows that at this location, the peak concentration for ^{131}I (1.9 MBq/m^3) is now lower than that for ^{137}Cs (2.56 MBq/m^3).

3.1.4 Low and High Tide

Figure 14 shows the simulated distribution for ^{137}Cs in the Scheldt estuary after 5 days for the start of the release at highest peak of the tide (Figure 14a) and at the lowest peak of the tide (Figure 14b). The distribution of radioactivity in the Scheldt estuary is similar whether the release occurs at high or low tide.

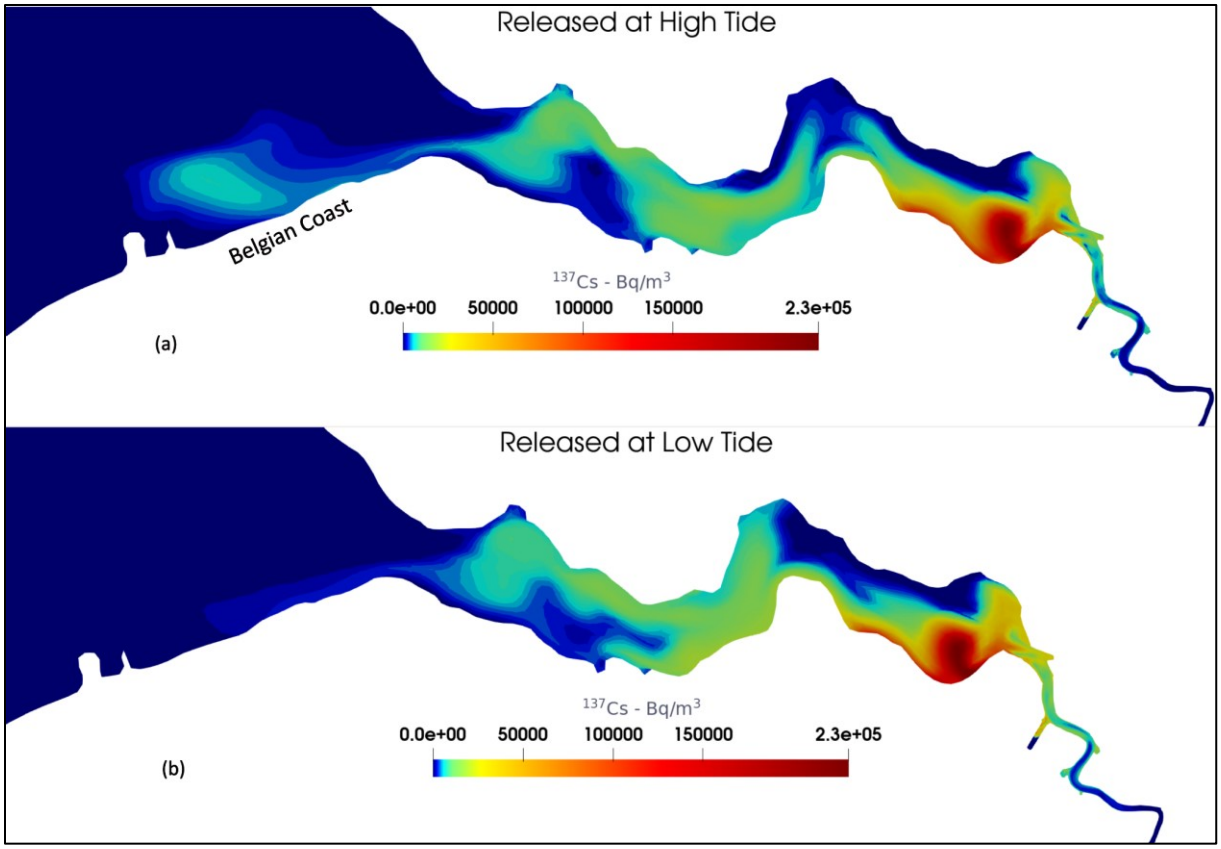

Figure 14. Simulated radioactivity distribution in the coast and the estuary for ^{137}Cs after 5 days of the initial release: the radioactive plume is released at the (a) high tide and (b) low tide condition at the location of NPP.

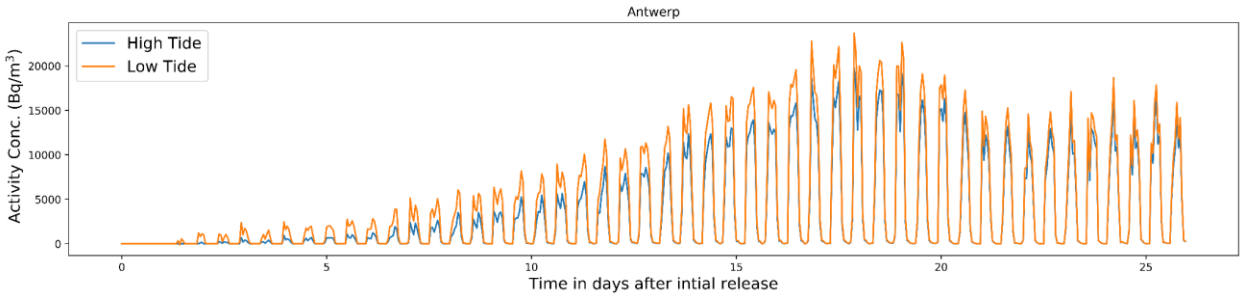

Figure 15. Temporal variation of radioactivity concentration for ^{137}Cs at Antwerp for release starting from low tide and high tide.

However, a small difference in peak concentrations (at high tide) can be observed at Antwerp (Figure 15), where the temporal variation for concentration follows the same trend except for the peak values. The peak values for the release at high tide are generally lower than those for releases at low tide. This is expected because Antwerp is located upstream of the release (no direct deposition here: see Figure 3 for scenario 1) and the plume released at low tide is transported towards the rivers, increasing the concentration. Furthermore, the difference in peak values is more prominent in the first few weeks, but after around 21 days, the peak values for both cases become similar.

The start of release at high tide has a greater impact on the coast than the release at low tide (Figure 14). However, for releases at high tide, the concentration along the coast does not exceed 7000 Bq/m^3, while released at low tide, no radioactivity is observed along the coast. Moreover, for scenario 1 (in Section 3.1.1), the radioactive contamination at the coast is lower than that observed here (for high tide). This is because the starting time of scenario 1 was chosen as the first hour of the first day of July, which corresponds to two hours after the high tide. Nonetheless, it should be noted that the increase in concentrations are less than 5%.

3.1.5 January and July

Figure 16 shows the distribution of ^{137}Cs in the Scheldt estuary after 5 days of simulation during the months of July (Figure 16a) and January (Figure 16b). In both cases the release period begins on the first day of their respective month.

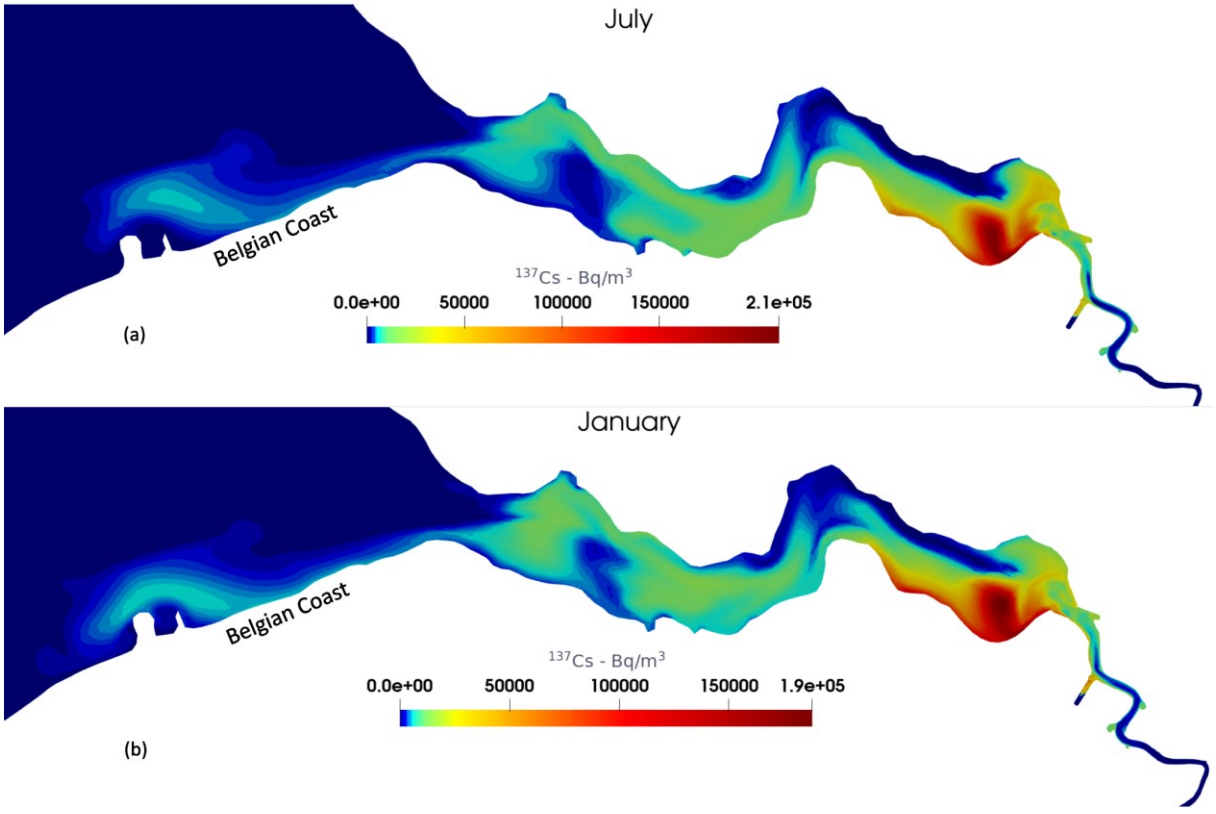

Figure 16. Simulated ^{137}Cs distribution in the coast and the estuary after 5 days of initial release for the month of (a) July and (b) January.

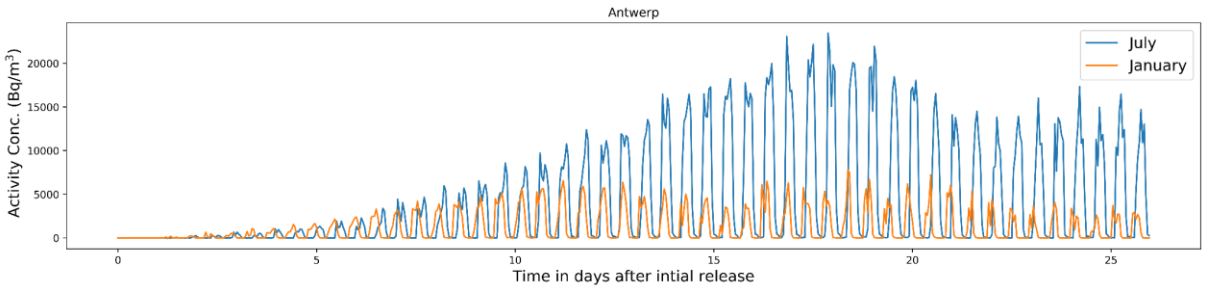

Figure 17. Temporal variation of radioactivity concentration for ^{137}Cs at Antwerp for the period of July and January.

After roughly 5 days, the concentrations obtained for July and January have a similar peak concentration of around 5000 Bq/m^3 at the coast (Figure 16). However, the distribution for each month shows a distinct spatial distribution. The most noticeable difference occurs in the lower estuary (lower estuary is represented in Figure 2) where the concentrations are lower for January than for July. Figure 17 shows the temporal variation of ^{137}Cs in Antwerp for the months of July and January. It can be seen here that after the initial week the concentration in July increases, whereas that in January remains lower. This is because of higher discharge from the river during January.

4 Conclusions

A hydrodynamic model was developed to simulate the fate of radionuclides in the Scheldt basin as a decision-support tool for emergency planning. The model has proved to be useful to simulate the spreading of radioactivity originated from both distributed (atmospheric releases) and point (direct releases) sources over any temporal scale. It provides valuable insight about the magnitude of activity concentration that could be found in this water system. The model includes the effect of wind drag and encloses a domain that covers the complete continental shelf region. This minimizes the impact of the boundary conditions on the calculations in the area of interest. The model has the capabilities to couple 1D and 2D domains with low computational cost. This characteristic is desirable in the case of emergency for faster diagnosis of the situation.

Irrespective of the release source (be it atmospheric or direct liquid releases), the tides in the estuary are the primary driving force in the distribution of radioactivity. Thus, the Scheldt estuary is the most vulnerable region where high activity concentrations are found for long periods. That is due to the constant change in direction induced by low and high tides. While the radioactivity at the Belgian coast is only seen for specific scenarios (atmospheric releases towards the sea). In the upstream parts of the river, the discharge plays a significant role in the upstream propagation and flushing of the radioactive plume. These interaction of the radioactivity between different flow regions (i.e. estuary-sea and river systems) is made possible by taking into account: (1) the impact of the tides and winds on radionuclide distribution in the complete system, (2) to consider the recirculation of the radioactive plume mainly along the coast, and (3) the seasonality (impact of variability of the river's discharge on the propagation of the plume in the upstream river system). In models restricted just to the area of interest around the NPP, the radioactive mass that leaves the domain is not taken into account. However, in tidal systems like Scheldt, radioactive plumes can return into the domain. Here, SLIM makes it possible to simulate a sufficiently large domain that keeps better track of the radioactive mass.

The model simulation for radioactivity distribution and its levels provides information for emergency responders to make informed decisions. For instance, even with such a large release amount, the results show that the impact on the Belgian coast is rather limited in space (within 35 km from the estuary mouth). Whereas for the deposition in rivers, the radioactivity level subsides within a few days. This can further aid in the effective planning of radioactivity measurements that need to be undertaken in the wake of an accident. Since tidal motions vary concentrations, the model can assist in foreseeing the time to observe maximum concentration. For instance,

measurements taken at low tide in Antwerp will provide extremely low radioactive levels. Subsequently, protective measures for the public can be implemented in areas with high radioactive concentrations. Additionally, with available projected data for discharge and tides, the model can support decisions by predicting the evolution of the radioactivity distribution in the event of a nuclear accident.

Acknowledgements: This research was carried out in the framework of doctoral fellowship PO4500049108, which is awarded to the first author of the present article and is funded by the Engie Electrabel and Belgian Nuclear Research Centre (SCK·CEN). The work was carried out in SCK·CEN and Université catholique de Louvain and the author is thankful for the resources provided. The authors are also grateful to Johan Camps (SCKCEN) for fruitful discussion regarding the scenarios and Katrijn Vandersteen (SCKCEN) for the providing the simulation results for the atmospheric deposition. The authors are also thankful for members of SLIM team that contributed to the development of the model.

References

Arndt, S., Vanderborght, J.-P., Regnier, P., 2007. Diatom growth response to physical forcing in a macrotidal estuary: Coupling hydrodynamics, sediment transport, and biogeochemistry. J. Geophys. Res. Oceans 112. https://doi.org/10.1029/2006JC003581

Behrens, E., Schwarzkopf, F.U., Lübbecke, J.F., Böning, C.W., 2012. Model simulations on the long-term dispersal of 137Cs released into the Pacific Ocean off Fukushima. Environ. Res. Lett. 7, 034004. https://doi.org/10.1088/1748-9326/7/3/034004

Bladé, E., Gómez-Valentín, M., Dolz, J., Aragón-Hernández, J.L., Corestein, G., Sánchez-Juny, M., 2012. Integration of 1D and 2D finite volume schemes for computations of water flow in natural channels. Adv. Water Resour. 42, 17–29. https://doi.org/10.1016/j.advwatres.2012.03.021

Breton, M., Salomon, J.C., 1995. A 2D long term advection-dispersion model for the Channel and Southern North Sea Part A: Validation through comparison with artificial radionuclides. J. Mar. Syst. 6, 495–513. https://doi.org/10.1016/0924-7963(95)00020-P

Brovchenko, I., Kim, K.O., Maderich, V., Jung, K.T., Bezhenar, R., Ryu, J.H., Min, J.E., 2022. Sediment and Radioactivity Transport in the Bohai, Yellow, and East China Seas: A Modeling Study. J. Mar. Sci. Eng. 10, 596. https://doi.org/10.3390/jmse10050596

Cao, Y., Lin, J., Zhai, K., Jiang, W., Zou, H., Ren, H., Wang, P., Gao, X., Zhang, M., Yu, S., Zhao, Y., Xuan, Z., Zhang, D., Liu, Y., Lou, X., 2022. Long-term investigation of environmental radioactivity levels and public health around the Qinshan Nuclear Power Plant, China. Sci. Rep. 12, 4945. https://doi.org/10.1038/s41598-022-09091-2

de Brye, B., de Brauwere, A., Gourgue, O., Kärnä, T., Lambrechts, J., Comblen, R., Deleersnijder, E., 2010. A finite-element, multi-scale model of the Scheldt tributaries, river, estuary and ROFI. Coast. Eng. 57, 850–863. https://doi.org/10.1016/j.coastaleng.2010.04.001

Draoui, I., Lambrechts, J., Legat, V., Deleersnijder, E., 2022. The discontinuous Galerkin method for coupling a 1D river model to a 2D shallow water one (No. EGU22-1084). Presented at the EGU22, Copernicus Meetings. https://doi.org/10.5194/egusphere-egu22-1084

Draoui, I., Lambrechts, J., Legat, V., Soares-Frazão, S., Hoitink, A.J.F., Deleersnijder, E., 2020. Discontinuous Galerkin method for 1D river flows. pp. 1114–1121. https://doi.org/10.1201/b22619-156

Egbert, G.D., Erofeeva, S.Y., 2002. Efficient Inverse Modeling of Barotropic Ocean Tides. J. Atmospheric Ocean. Technol. 19, 183–204. https://doi.org/10.1175/1520-0426(2002)019<0183:EIMOBO>2.0.CO;2

Eke, C.D., Anifowose, B., Van De Wiel, M.J., Lawler, D., Knaapen, M.A.F., 2021. Numerical Modelling of Oil Spill Transport in Tide-Dominated Estuaries: A Case Study of Humber Estuary, UK. J. Mar. Sci. Eng. 9, 1034. https://doi.org/10.3390/jmse9091034

Estournel, C., Bosc, E., Bocquet, M., Ulses, C., Marsaleix, P., Winiarek, V., Osvath, I., Nguyen, C., Duhaut, T., Lyard, F., Michaud, H., Auclair, F., 2012. Assessment of the amount of cesium-137 released into the Pacific Ocean after the Fukushima accident and analysis of its dispersion in Japanese coastal waters. J. Geophys. Res. Oceans 117. https://doi.org/10.1029/2012JC007933

Hersbach, H., Bell, B., Berrisford, P., Hirahara, S., Horányi, A., Muñoz-Sabater, J., Nicolas, J., Peubey, C., Radu, R., Schepers, D., Simmons, A., Soci, C., Abdalla, S., Abellan, X., Balsamo, G., Bechtold, P., Biavati, G., Bidlot, J., Bonavita, M., Chiara, G., Dahlgren, P., Dee, D., Diamantakis, M., Dragani, R., Flemming, J., Forbes, R., Fuentes, M., Geer, A., Haimberger, L., Healy, S., Hogan, R.J., Hólm, E., Janisková, M., Keeley, S., Laloyaux, P., Lopez, P., Lupu, C., Radnoti, G., Rosnay, P., Rozum, I., Vamborg, F., Villaume, S., Thépaut, J., 2020. The ERA5 global reanalysis. Q. J. R. Meteorol. Soc. 146, 1999–2049. https://doi.org/10.1002/qj.3803

Hossen, M.A., Akhter, F., 2015. Study Of the Wind Speed, Rainfall And Storm Surges For The Scheldt Estuary In Belgium. International Journal of Scientific & Technological Research 4.

IAEA, 2019. Modelling of Marine Dispersion and Transfer of Radionuclides Accidentally Released from Land Based Facilities (No. IAEA-TECDOC-1876). International Atomic Energy Agency.

IAEA, 2006a. Radiological Conditions in the Dnieper River Basin. International Atomic Energy Agency, Vienna.

IAEA, 2006b. Environmental Consequences of the Chernobyl Accident and their Remediation: Twenty Years of Experience. International Atomic Energy Agency, Vienna.

Ievdin, I.O., Khalchenkov, O.V., Kovalets, I.V., Raskob, W., Trybushnyi, D., Zheleznyak, M.J., 2012. Application of Decision Support System JRODOS for Assessments of Atmospheric Dispersion and Deposition from Fukushima Daiichi Nuclear Power Plant Accident. Int. J. Energy Clean Environ. 13. https://doi.org/10.1615/InterJEnerCleanEnv.2013006151

Kärnä, T., Baptista, A.M., Lopez, J.E., Turner, P.J., McNeil, C., Sanford, T.B., 2015. Numerical modeling of circulation in high-energy estuaries: A Columbia River estuary benchmark. Ocean Model. 88, 54–71. https://doi.org/10.1016/j.ocemod.2015.01.001

Kawamura, H., Kobayashi, T., Furuno, A., In, T., Ishikawa, Y., Nakayama, T., Shima, S., Awaji, T., 2011. Preliminary numerical experiments on oceanic dispersion of 131I and 137Cs discharged into the ocean because of the Fukushima Daiichi nuclear power plant disaster. J. Nucl. Sci. Technol. 48, 1349–1356. https://doi.org/10.3327/jnst.48.1349

Kobayashi, T., Nagai, H., Chino, M., Kawamura, H., 2013. Source term estimation of atmospheric release due to the Fukushima Dai-ichi Nuclear Power Plant accident by

atmospheric and oceanic dispersion simulations. J. Nucl. Sci. Technol. 50, 255–264. https://doi.org/10.1080/00223131.2013.772449
Kovalets, I.V., Robertson, L., Persson, C., Didkivska, S.N., Ievdin, I.A., Trybushnyi, D., 2014. Calculation of the far range atmospheric transport of radionuclides after the Fukushima accident with the atmospheric dispersion model MATCH of the JRODOS system. Int. J. Environ. Pollut. 54, 101–109. https://doi.org/10.1504/IJEP.2014.065110
Lacroix, G., Ruddick, K., Ozer, J., Lancelot, C., 2004. Modelling the impact of the Scheldt and Rhine/Meuse plumes on the salinity distribution in Belgian waters (southern North Sea). J. Sea Res. 52, 149–163. https://doi.org/10.1016/j.seares.2004.01.003
Park, S.-U., Lee, I.-H., Joo, S.J., Ju, J.-W., 2017. Emergency preparedness for the accidental release of radionuclides from the Uljin Nuclear Power Plant in Korea. J. Environ. Radioact. 180, 90–105. https://doi.org/10.1016/j.jenvrad.2017.09.012
Patil, A., Perez, F., Lambrechts, J., Draoui, I., Deleersnijder, E., 2022. Numerical modelling of navigable rivers: influence of navigation structures on the Meuse River flow, in: Proceedings of the 11th International Conference on Fluvial Hydraulics. Presented at the River flow 2022, Taylor and Francis, Kingston and Ottawa, Canada. https://doi.org/10.1201/9781003323037-86
Periáñez, R., Bezhenar, R., Brovchenko, I., Duffa, C., Iosjpe, M., Jung, K.T., Kim, K.O., Kobayashi, T., Liptak, L., Little, A., Maderich, V., McGinnity, P., Min, B.I., Nies, H., Osvath, I., Suh, K.S., de With, G., 2019. Marine radionuclide transport modelling: Recent developments, problems and challenges. Environ. Model. Softw. 122, 104523. https://doi.org/10.1016/j.envsoft.2019.104523
Periáñez, R., Cortés, C., 2023. A Numerical Model to Simulate the Transport of Radionuclides in the Western Mediterranean after a Nuclear Accident. J. Mar. Sci. Eng. 11, 169. https://doi.org/10.3390/jmse11010169
Periáñez, R., Min, B.I., Suh, K.S., 2021. The transport, effective half-lives and age distributions of radioactive releases in the northern Indian Ocean. Mar. Pollut. Bull. 169, 112587. https://doi.org/10.1016/j.marpolbul.2021.112587
Prandle, D., Charnock, H., 1997. A modelling study of the mixing of 137Cs in the seas of the European Continental Shelf. Philos. Trans. R. Soc. Lond. Ser. Math. Phys. Sci. 310, 407–436. https://doi.org/10.1098/rsta.1984.0002
Raskob, W., Landman, C., Trybushnyi, D., 2016. Functions of decision support systems (JRodos as an example): overview and new features and products. Radioprotection 51, S9–S11. https://doi.org/10.1051/radiopro/2016015
Reynaud, J.-Y., Witt, C., Pazmiño, A., Gilces, S., 2018. Tide-dominated deltas in active margin basins: Insights from the Guayas estuary, Gulf of Guayaquil, Ecuador. Mar. Geol. 403, 165–178. https://doi.org/10.1016/j.margeo.2018.06.002
Selivanova, A., Hůlka, J., Kotík, L., Kuča, P., Rubovič, P., Malátová, I., Helebrant, J., Koc, J., Rulík, P., Vlček, O., 2023. Advanced simulation techniques for the transport of routine atmospheric discharges using the JRODOS system. Prog. Nucl. Energy 157, 104596. https://doi.org/10.1016/j.pnucene.2023.104596
Tsabaris, C., Eleftheriou, G., Tsiaras, K., Triantafyllou, G., 2022. Distribution of dissolved 137Cs, 131I and 238Pu at Eastern Mediterranean Sea in case of hypothetical accident at the Akkuyu Nuclear Power Plant. J. Environ. Radioact. 251–252, 106964. https://doi.org/10.1016/j.jenvrad.2022.106964

Tsumune, D., Tsubono, T., Aoyama, M., Hirose, K., 2012. Distribution of oceanic 137Cs from the Fukushima Dai-ichi Nuclear Power Plant simulated numerically by a regional ocean model. J. Environ. Radioact., Environmental Impacts of the Fukushima Accident (Part I) 111, 100–108. https://doi.org/10.1016/j.jenvrad.2011.10.007

Tsuruta, H., Oura, Y., Ebihara, M., Ohara, T., Nakajima, T., 2014. First retrieval of hourly atmospheric radionuclides just after the Fukushima accident by analyzing filter-tapes of operational air pollution monitoring stations. Sci. Rep. 4, 6717. https://doi.org/10.1038/srep06717

UNSCEAR, 2021. Levels and effects of radiation exposure due to the accident at the Fukushima Daiichi Nuclear Power Station: implications of information published since the UNSCEAR 2013 Report. United nations.

van Rijn, L.C., 2013. Tidal phenomena in the Scheldt Estuary, part 2. Deltares.

Wang, J., Baskaran, M., Cukrov, N., Du, J., 2022. Geochemical mobility of 137Cs in marine environments based on laboratory and field studies. Chem. Geol. 614, 121179. https://doi.org/10.1016/j.chemgeo.2022.121179